Available online at www.sciencedirect.com

ScienceDirect

www.elsevier.com/locate/jes

JES JOURNAL OF ENVIRONMENTAL SCIENCES

www.jesc.ac.cn

Characterization of $Fe_5(AsO_3)_3Cl_2(OH)_4{\cdot}5H_2O$, a new ferric arsenite hydroxychloride precipitated from $FeCl_3$–As_2O_3–HCl solutions relevant to arsenic immobilization

Zidan Yuan [1], *Xu Ma* [1,2], *Xing Wu* [1], *Guoqing Zhang* [1,2], *Xin Wang* [1], *Shaofeng Wang* [1,*], *Yongfeng Jia* [1,*]

[1] *Key Laboratory of Pollution Ecology and Environmental Engineering, Institute of Applied Ecology, Chinese Academy of Sciences, Shenyang 110016, China*

[2] *University of Chinese Academy of Sciences, Beijing 100049, China*

ARTICLE INFO

Article history:
Received 24 September 2019
Received in revised form
12 December 2019
Accepted 12 December 2019
Available online 26 December 2019

Keywords:
Chloride ion
Acidic pH
Ferric arsenite hydroxychloride
Characterization
Immobilization

ABSTRACT

Tooeleite ($Fe_6(AsO_3)_4SO_4(OH)_4{\cdot}4H_2O$) is widely precipitated for direct As(III) removal from sulfate-rich industrial effluents. However, whether or not Fe(III)–As(III)–Cl(-I) precipitate is produced in chloridizing leaching media for As immobilization is almost unknown. This work founded the existence of ferric arsenite (hydroxy)chloride as a new mineral for As(III) removal. Its chemical composition and solid characterization were subsequently studied by using scanning electron microscope with an energy dispersive spectrometer (SEM-EDS), X-ray diffraction (XRD), infrared (FT-IR), Raman spectroscopy and thermogravimetric (TG) curve. The results showed the formation of a yellow precipitate after 3-days reaction of Fe(III)/As(III) with molar ratio ≈ 1.7 in chloride solution at pH 2.3 neutralized with NaOH. Compared with tooeleite, chemical analysis and solid characterization indicated that Cl(-I) replaces SO_4(-II) producing ferric arsenite hydroxychloride with formula $Fe_5(AsO_3)_3Cl_2(OH)_4{\cdot}5H_2O$. This new plate shaped solid showed better crytallinity than tooeleite, although it has similar morphology and characteristic bands to tooeleite. The FT-IR bands at 628, 964 cm^{-1} and the Raman bands at 448, 610, 961 cm^{-1} were assigned to Fe–O or As(III)–O–Fe or As(III)–O bending/stretching vibration, indicating that both arsenite and chloride substituted for the position of sulfate for ferric arsenite hydroxychloride produced due to the lack of the SO_4^{2-} vibrations. Cl-(I) also contributed to increase As removal efficiency in aqueous sulfate media under acidic pH conditions via the probable formation of sulfate-chloride ferric arsenite.

* *Corresponding authors.*
E-mail addresses: wangshaofeng@iae.ac.cn (S. Wang), yongfeng.jia@iae.ac.cn (Y. Jia).

https://doi.org/10.1016/j.jes.2019.12.009

Introduction

Arsenic contamination in water body from industrial activities is a worldwide environmental issue (Azamat et al., 2018; Halder et al., 2018). The application of metallurgy of metal concentrates generated a great quantity of high arsenic-bearing acidic wastewater (Revesz et al., 2016).

In the process of acid leaching, arsenic occurs largely as arsenate (As(V)) and arsenite (As(III)). Chemical precipitation is widely employed in the treatment of arsenic-rich waste acid. As(V) is directly removed from the effluents to sub-ppm level by (co)precipitation with ferric salts under strong acid pH for ferric arsenate/scorodite and under near-neutral pH for Fe(III)–As(V) co-precipitate (Ma et al., 2019; Nur et al., 2019; Zhang et al., 2019). More toxic As(III) can often be efficiently captured by its pre-oxidation to As(V) as the basis of following (co)precipitation processes due to its higher mobility and solubility (Zhang et al., 2011; Okibe et al., 2014). As(III) can be oxidized to As(V) by various As(III) oxidizing agents including hydrogen peroxide solution (H_2O_2), Fenton/Fenton-like reagent (Fe(II)+H_2O_2/O_2), permanganate (MnO_4^-) and As-oxidizing bacteria (Zhang et al., 2011; Cai et al., 2019; Yuan et al., 2019). However, disposal costs and/or time-consumption are influenced negatively by the addition of abiotic As(III) oxidizers and microbial incubation. Therefore, the cost-effective and time-saving As(III) removal from metallurgical effluents presents more challenging.

The direct As(III) removal without the biotic/abiotic As(III) oxidizing operations has been paid more attention recently. Previous studies show that the direct removal of As(III) is feasible in conditional iron salt precipitation methods. As(III) associated with mix-valence iron (Fe(II,III)) and/or other metal cations (e.g. Pb, Ti) can produce arsenite solids including schneiderhöhite ($(Fe(II)Fe(III)_3As_5O_{13})$), fetiasite ($((Fe(II),Fe(III),Ti)_3[As_2O_5]O_2$) and ludlockite ($PbFe(III)_4As_{10}O_{22}$) (Ledderboge et al., 2014; Sancho-Tomás et al., 2018). As(III) can also combine with Fe(III) to form tooeleite in aqueous sulfate media including acid mine drainage and sulphuric acid leaching systems (Majzlan et al., 2016; Chai et al., 2018). This ferric arsenite hydroxy-sulfate has been found at pH 1.8–4 and >0.5 g/L of initial As concentrations (Chai et al., 2016). It is noted, however, that not all hydrometallurgical effluents contain sulfate. For some oxyacid salts minerals (e.g. barite, malachite, augite, etc), chloridizing leaching is employed instead of sulphuric acid leaching to effectively enhance metal recovery according to the higher solubilities of most metal chlorides (Michelis et al., 2013). Chlorine ion (Cl(-I)) from the chloridizing extraction reagents including hydrochloric acid and chlorides is one of the main components in hydrometallurgical wastewater (Michelis et al., 2013; Zhou et al., 2016). Hence it is necessary to investigate the influence of Cl(-I) on direct As(III) removal.

Magnussonite ($Mn_{10}As_6O_{18}Cl(OH)$) and finnemanite ($Pb_5(AsO_3)_3Cl$) as natural minerals indicate that Cl(-I) can incorporate into the structure and composition of some metal arsenites (Bahfenne and Frost, 2010; Priestner et al., 2019). Furthermore, Cl(-I) can also act as the intercalated anion involving the formation of chloride green rust ($(Fe(II)_3Fe(III)(OH)_8Cl\cdot 2H_2O$) via precipitation from $FeCl_2$–$FeCl_3$ mixed solution at Fe(II)/Fe(III) molar ratio of 3 at pH 7–8 neutralized with NaOH (Maithreepala and Doong., 2005; Alidokht et al., 2016). Few studies, however, have examined the (co)precipitate forms in the Fe(III)–As(III)–Cl(-I) system to date. Cl(-I) occurrence in the metallurgical wastewater may produce chloride ferric arsenite, which is likely to be a new sink for direct As(III) fixation.

The aim of this paper is to study whether Cl(-I) associates with Fe(III)–As(III) (co)precipitate for the formation of ferric arsenite (hydroxy)chloride or not. Neutralization-precipitation of As(III) with Fe(III) in aqueous chloride media is investigated at various pH values, because the formation of Fe–As (co)precipitates currently discovered is strongly pH dependent. If so, the pH condition for the precipitate, the chemical composition of this solid and its solid characterization will be determined. For effective As(III) removal in acid mine drainage and sulphuric acid leaching systems, the effect of Cl(-I) on As(III) mobilization in aqueous sulfate media is also studied over a wide range of pH. This study can provide the reference for the wide application of Cl(-I) on the treatment of As(III)-rich wastewater.

1. Materials and methods

This experiment was performed at room temperature (25°C) inside a glove box and under the strict anaerobic conditions where high-purity N_2 was used to avoid As(III) oxidation. Fresh deoxygenated de-ionized water (DI-water) was prepared by boiling DI-water for 1 h and cooling under the N_2. Analytical grade $FeCl_3\cdot 6H_2O$ and As_2O_3 were purchased from the Sinopharm Group Chemical Reagent Co., Ltd. and Hunan Province Shuikoushan mining bureau of the Hengyang industrial company, respectively. Fe(III) and As(III) stock solutions were prepared by dissolving $FeCl_3\cdot 6H_2O$ and As_2O_3 into dilute hydrochloric acid at pH 0.8, respectively.

1.1. *Precipitation procedure in chloride media*

There is no a fixed value determined for the molar ratio of Fe/As/Cl in actual metallurgical effluents after the chloridizing leaching. For rational use of Fe(III) salts, the Fe/As molar ratio in this work was set to 1.5–2. Equal volumes of 10.71 mmoL/L Fe(III) and 6.13 mmoL/L As(III) mixed solutions were adjusted to pH 1.6, 1.9, 2.3, 2.6, 3.0, 4.5, 5.3, 6,2, 7.1 and 9.5 by adding 1 moL/L NaOH and constant-volumed to 50 mL in serum bottles. The solutions/suspensions were maintained under vigorously stirring for 3 days. The initial concentrations of Fe(III), As(III) and Cl(-I) in all systems were 600, 460 and 1350 mg/L, respectively. 2 mL of the mixtures were collected at regular time intervals and then filtered through 0.1 μm membrane filters for the analysis of the concentrations of Fe(III), As(III) and Cl(-I) remaining. All tests were conducted in duplicates and the averages were reported.

The residual solids after 0.5, 1 and 3 days' reactions were washed three times with deoxygenated DI-water to remove the entrained solution among the particles and inorganic salt (e.g. NaCl). Then the solids were dried naturally, ground in the glove box under N_2, and stored in serum bottles with a butyl rubber stopper for later characterization.

1.2. Synthesis of reference materials

Ferric arsenite hydroxysulfate was synthesized according to the method described previously (Chai et al., 2016). Briefly, ferric iron solution ($Fe_2(SO_4)_3 \cdot 5H_2O$) and arsenite solution (As_2O_3) were adjusted to pH 0.8 using H_2SO_4, respectively. The Fe(III)–As(III) mixed solution at desired Fe/As molar ratio of 1.5 was neutralized with NaOH solution to pH 2. The mixture was then stabilized for 0.5 and 1 day under magnetic stirring. The orange and yellow precipitates after 0.5 and 1 day reactions separately identified using X-ray diffraction (XRD).

1.3. Analysis of arsenic, iron and chloride concentrations

As(III) and As Total (As(T)) concentrations were measured according to the method described previously via a hydride generation-atomic fluorescence spectrometry (AFS-2202E, KCHG, China) with a detection limit of 0.1 μg/L using 0.5 moL/L disodium citrate buffer and 5% HCl as carrier solutions (Xiao et al., 2015; Yuan et al., 2019). Fe Total (Fe(T)) concentration was analyzed by a flame atomic absorption spectrophotometer (AA240, Varian, USA) in the presence of 5% HNO_3 with the detection limit of 0.05 mg/L. The concentration of chloride was determined by an ion chromatograph (DIONEX ICS-1100, Thermo Fisher Scientific, USA). Origin 8.0 software was used for data analysis and graphing.

1.4. Characterization methods

At the end of precipitation reactions, all solids were rinsed three times with deoxygenated DI-water, naturally dried and then ground in the anaerobic glove box under N_2 for further analyses.

The morphology, elemental composition and distribution of the solid samples coated with a thin gold layer were done on a scanning electron microscope with an energy dispersive spectrometer (SEM-EDS, Quanta 250, FEI, USA) under high vacuum at 30 kV.

The XRD analysis of powder samples was performed with an X-ray diffractometer (D/max 2000 PC, Rigaku, Japan) equipped with a copper target ($\lambda = 1.5418$ Å) at 56 kV and 182 mA in step-scanning range of 5–80° 2θ and a step size of 0.02° 2θ. Jade 6.5 software was used to assist in XRD result analysis.

Infrared spectra (FT-IR) of produced precipitates over the range of 400–4000 cm^{-1} were obtained by a Fourier transform infrared spectrometer (Nicolet 6700, Thermo Fisher Scientific, USA) using Omnic 9.0 software with the co-addition of 200 scans and a resolution of 4 cm^{-1}. The mixtures of 0.5% subsamples and 99.5% KCl were finely ground in order to prepare thin slices using a tablet press.

Raman spectra from 200 to 1000 cm^{-1} was conducted on a Raman microscope (DXR, Thermo Fisher Scientific, USA) using Omnic 9.0 software with the 10× objective and a He–Ne laser operating at 780 nm operating at 0.8 mW laser power, 25 μm slit aperture, 400 lines/mm grating, 20 min scans and 4.4 cm^{-1} band resolution.

The number of crystallization waters was determined by a Thermal gravimetric (TG) analyzer (Q50, TA, USA) in the temperature range of 20–800°C at a heating rate of 10°C/min. The purge gas used was nitrogen at gas flow rate of 60 mL/min.

1.5. Precipitation of As(III) with Fe(III) in aqueous sulfate-chloride media

The effects of Cl(-I) on arsenic removal in aqueous sulfate media at various pH values were evaluated by using As_2O_3 with $Fe_2(SO_4)_3 \cdot 5H_2O$ instead of $FeCl_3 \cdot 6H_2O$ for Fe(III)–As(III) mixed solution. As(III) and Fe(III) solutions were adjusted to pH 0.8 using diluted hydrochloric acid. The same initial concentrations of Fe(III) and As(III) and pH conditions were applied as the corresponding Fe(III)–As(III)–Cl(-I) systems. As(III) removal in aqueous sulfate media in the absence of Cl(-I) is used as controlled trials. All tests were conducted in duplicates and the averages were reported.

1.6. Toxicity characteristic leaching procedure (TCLP) tests of the ferric arsenite hydroxychloride and tooeleite

The TCLP test was performed to evaluate the stability of toxic solid wastes disposed in the environment by leaching solid samples and analyzing the concentrations of dissolved toxic elements. After the treatment of As removal, the precipitated samples were vacuum pre-dried to constant weight at 105°C. For the extracted solution, 5.7 mL of glacial acetic acid and 500 mL of DI-water were added into 64.3 mL of 1 moL/L NaOH solution, then the pH of mixed solution was maintained at 4.93 ± 0.05 using 1 moL/L NaOH with a final volume of 1 L. 0.5 g of two obtained solid samples (ferric arsenite hydroxychloride and tooeleite) were separately leached by acetate buffer solutions at 23 ± 2°C for 18 ± 2 hr in 10 mL centrifuge tubes, with the liquid/solid ratio of 20:1 (mL/g) and agitation speed of 30 ± 2 r/min.

2. Results and discussion

2.1. Precipitation of As(III) with Fe(III) in aqueous chloride media

Fig. 1 shows the effect of pH on the precipitation of As(III) with Fe(III) in the presence of Cl(-I). After 3-days reaction, the Fe(III) and As(III) concentrations in aqueous phases over the pH range of 1.6–9.5 presented the trend of declining-rising-declining, but as a whole, both the concentrations of Fe(III) and As(III) were falling.

The concentrations of Fe(III) and As(III) were nearly constant at pH 1.6–1.9, indicating the formation of little precipitate. The first valley appeared at pH 2.3, with the Fe(III) 419.1 mg/L and As(III) 296.6 mg/L, indicating that 30.2% Fe(III) and 35.5% As(III) were immobilized in the solid phase probably mainly as a Fe(III)–As(III) precipitate at Fe/As molar ratio of 1.48 ± 0.20. This is because the ability of Fe(III) hydrolysis is low at pH 2.3 (Stefansson et al., 2007) and As(III) as H_3AsO_3 cannot be coprecipitated with or adsorbed onto Fe(III) hydroxide (e.g. ferrihydrite) at the Fe(III)/As(III) molar ratio of <2 (Jain and Loeppert, 2000; Kobya et al., 2020). The concentrations of Fe(III) and As(III) suddenly increased at pH 2.6. This phenomena is probably due to that the strong competition

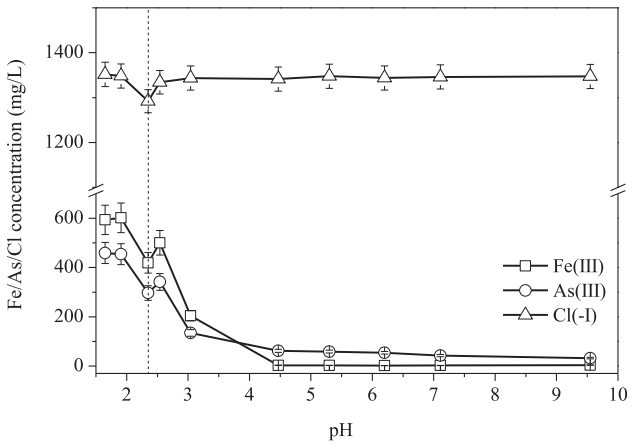

Fig. 1 – The concentrations of Fe(III), As(III) and Cl(-I) in solution as a function of pH after 3-days precipitation reaction in aqueous chloride media. Data are represented as averages ± standard deviation.

between AsO_3^{3-} and OH^- for Fe^{3+}inhibited the accumulation of both ferric arsenite and Fe(III) hydroxide on the solid phase. Fe(III) concentration subsequently reached a plateau at pH 4.5 because of complete hydrolysis of Fe(III), whereas the As(III) concentration decreased consistently until it reached the minimum value (32.0 mg/L) at pH 9.5. This is due to the strong affinity between Fe(III) hydroxide and arsenite at higher pH levels. Furthermore, Cl(-I) could be associated with the Fe(III)–As(III) precipitate at pH 2.3 and As(III)/Cl(-I) molar ratio of 1.33 ± 0.20 according to the obvious decrease of aqueous Cl(-I).

The color of remained solutions or slurries is changed with increasing pH (Appendix A Fig. S1a). Bright yellow solution was transformed into yellow precipitate when pH increased from 1.9 to 2.3, which was similar to the color of synthetic tooeleite with the reaction time of 3 days (Chai et al., 2016). The color of slurries changed from orange at pH 2.6 to reddish brown at pH 3.0–9.5, which reasonably indicated the formation of ferrihydrite.

2.2. *Characterization studies*

Due to Fe(III) hydrolysis, the mixture of amorphous Fe(III)–As(III)–Cl(-I) precipitate and As(III)-bearing ferrihydrite as the solid product at pH > 2.3 (Appendix A Fig. S2) was not conducive to confirm the chemical formula of ferric arsenite hydroxychloride. Therefore, only the characterization of the obtained solid at pH 2.3 was reported.

2.2.1. *SEM-EDS*

The morphology of Fe(III)–As(III)–Cl(-I) precipitate at pH 2.3 together with EDS and element mapping analysis for Fe, As, Cl and O are shown in Fig. 2, Appendix A Fig. S3 and Table 1. The synthesized Fe(III)–As(III)–Cl(-I) precipitate existed as plate shaped crystallites with the size ≤ 1 μm. This was similar to the configuration of tooeleite crystal (Morin et al., 2003; Chai et al., 2018). No spherical cluster was observed in this work. The Fe:As:Cl molar ratio of the precipitate was 5:3:2 as indicated by the mean EDS quantitative results, which was very close to the ratio of the above-mentioned chemical analysis. The results of element mapping reconfirmed that the final solid at pH 2.3 was reasonably homogeneous and consists of Fe, As, Cl and O.

2.2.2. *XRD*

The reaction products of As(III) with Fe(III) in chloride solution at pH 2.3 under different reaction time were characterized by XRD and their patterns are compared with those of ferric arsenite hydroxysulfate and tooeleite in Fig. 3. The synthesized ferric arsenite hydroxysulfate was partially crystallined after 0.5-day reaction and its XRD patterns were dominated by those of tooeleite. After 1-day reaction, this solid showed very good crystallinity and the diffraction lines corresponded to those of tooeleite ($Fe_6(AsO_3)_4SO_4(OH)_4\cdot 4H_2O$ PDF 44–1468).

In the Fe(III)–As(III)–Cl(-I) system, the XRD spectrum of the solid obtained at pH 2.3 within 0.5-day reaction showed two broad bands at 29° and 59° 2θ and located at the similar positions to those of poorly crystalline ferric arsenate (28° and 58° 2θ), indicating the formation of amorphous Fe(III)–As(III) co-precipitate. This amorphous phase subsequently converted to the crystalline state of Fe(III)–As(III)–Cl(-I) precipitateafter 1 day reaction, which suggested the slower crystallization process comparing with the formation of tooeleite. After 3-days reaction, the good crystallinity of Fe(III)–As(III)–Cl(-I) precipitate was obtained and its XRD pattern containing ten diffraction peaks at 10°, 20°, 26°, 28°, 30°, 33°, 36°, 43°, 53°, and 57° 2θ, which were matched closely with those of tooeleite. It indicated that Cl(-I) was very likely to be substituted for SO_4(-II) to form ferric arsenite hydroxychloride, hence yielded the structural formula $Fe_5(AsO_3)_3Cl_2(OH)_4\cdot nH_2O$ with Fe:As:Cl molar ratio 5:3:2. A fraction of the water content in this formula was assigned as OH for charge balance purposes. The number of crystallization water need to be further determined.

2.2.3. *FT-IR*

The infrared spectrum of ferric arsenite hydroxychloride was compared with that of tooeleite (Fig. 4). The bands of two solids between 1800 and 4000 cm^{-1}, known as the OH stretching region of adsorbed and structural H_2O were almost the same. Hence, only the frequency region of interest mainly including Fe–O, As(III)–O, structural SO_4^{2-} and adsorbed water of tooeleite were displayed. For tooeleite, the overlapping bands at 509 cm^{-1} were assigned to symmetric bending mode of SO_4^{2-} (Liu et al., 2013; Chai et al., 2016) and lattice Fe–O mode (Peulon et al., 2003), while the strong feature at 620 cm^{-1} was attributed to antisymmetric bending mode of SO_4^{2-}. A weak intense band observed at 769 cm^{-1} was ascribed to As(III)–O stretching vibration (Liu et al., 2013; Chai et al., 2016). The vibrations of the higher wave numbers at 983 and 1097 cm^{-1} corresponded to sorbed SO_4^{2-} symmetric and outer sphere bound SO_4^{2-} antisymmetric stretching vibrations, respectively. The adsorption band at 1637 cm^{-1} was readily attributed to be the bending vibration of adsorbed water.

The infrared spectrum of crystalline ferric arsenite hydroxychloride showed more adsorption bands in the region of the lower wave numbers after 3-days reaction. Two well resolved lattice Fe–O vibration bands at 474 and 512 cm^{-1} were clearly seen (Peulon et al., 2003), because the SO_4^{2-}

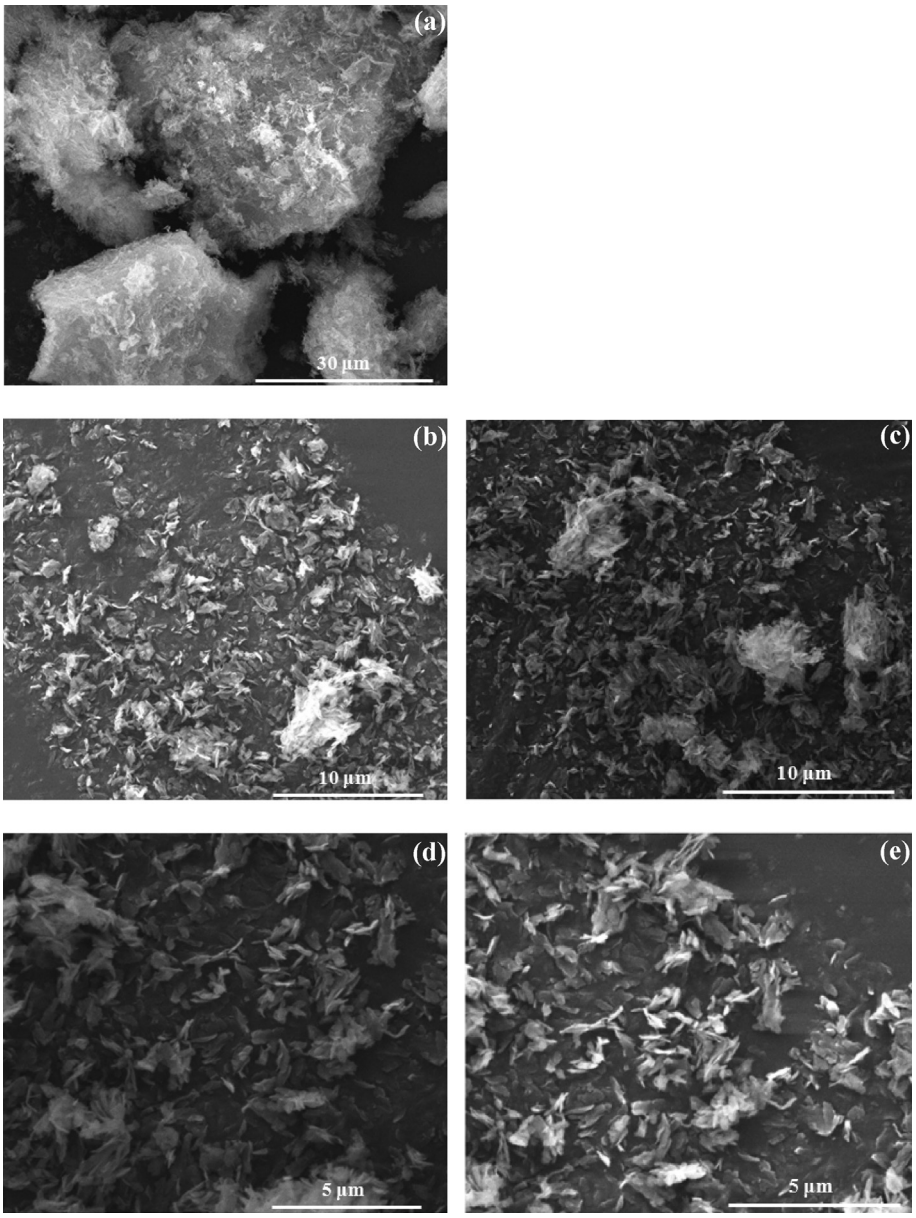

Fig. 2 – SEM images of the solid obtained at pH 2.3 with 2000, 5000 and 10,000 magnifications from (a)–(e). SEM image at 2000 magnification for the element mapping images of the final solid at pH 2.3 including Fe, As, Cl and O from (a1)-(a4).

symmetric bending mode band at the similar position no longer existed and cannot obscured the relatively weak signal of the Fe–O modes. A new band of crystalline ferric arsenite hydroxychloride at 551 cm^{-1} was reasonably assigned to Fe–O symmetric stretching vibration, which was located at the similar position to that of Fe_3O_4 (Yew et al., 2016). Compared with SO_4^{2-} antisymmetric bending mode band of tooeleite, the infrared band of crystalline ferric arsenite hydroxychloride at 628 cm^{-1} was very likely due to Fe–O antisymmetric stretching vibration. It was in line with the Fe–O stretching vibration in goethite (Gotić and Musić, 2007). Another new band at 694 cm^{-1} for crystalline ferric arsenite hydroxychloride was considered to be due to the As(III)–O–Fe(III) stretching vibration according to the observation in Fe(III)–As(III) co-precipitate (Müller et al., 2010). The bands observed at 777 and 964 cm^{-1} were attributed to As(III)–O stretching vibrations. These results were in agreement with the previous work (Müller et al., 2010). The adsorbed water of crystalline ferric arsenite hydroxychloride was characterized by bending bands at 1616 cm^{-1} according to the band at 1637 cm^{-1} in tooeleite.

2.2.4. *Raman*

The Raman spectra of tooeleite and crystalline ferric arsenite hydroxychloride are compared in Fig. 5. In the lower wave numbers region from 100 to 300 cm^{-1}, both tooeleite crystalline and crystalline ferric arsenite hydroxychloride showed four stronger bands at 127–128, 165–166, 193–197 and 272-278 cm^{-1}, which were assigned to As–O lattice vibrations

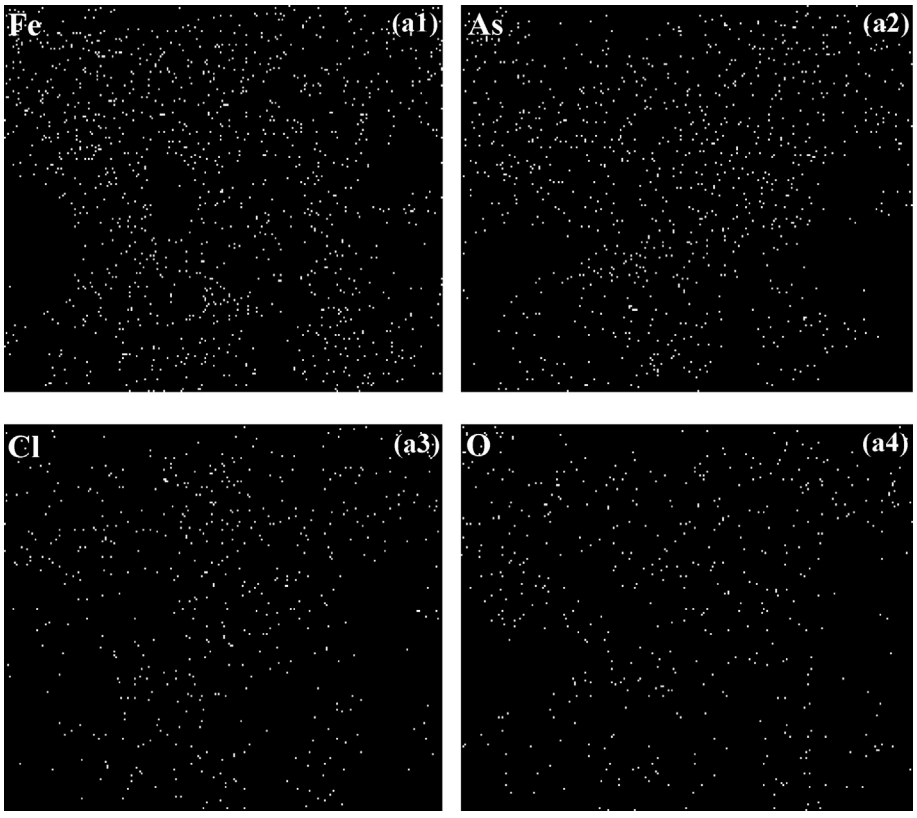

Fig. 2 – (*continued*).

(Frost et al., 2003; Makreski et al., 2015). A relatively weak band at 363/360 cm^{-1} and strong band at 507/503 cm^{-1} in two solids was attributed to the As–O in-plane and out-of-plane bending vibrations, respectively (Frost et al., 2003).

The difference of suggested peak assignment between tooeleite and crystalline ferric arsenite hydroxychloride was observed by five bands at 448–451, 604–610, 660–661, 780–806 and 961-980 cm^{-1}. For tooeleite, the three bands at 451, 604 and 980 cm^{-1} were assigned to the SO_4^{2-} doubly degenerate symmetric bending, triply degenerate antisymmetric bending and non-degenerate symmetric stretching vibrations (Liu et al., 2013). Previous work indicated that peak deconvolution of the band at 780 cm^{-1} generated two bands at 758 and 803 cm^{-1}. That together with another band at 660 cm^{-1} were due to the As(III)–O antisymmetric and symmetric stretching vibrations and As(III)–OH stretching vibration (Müller et al., 2010; Liu et al., 2013).

Table 1 – Elemental composition of the final solid at pH 2.3 as indicated by the energy dispersive spectrometer from scanning electron microscope (SEM) areas shown in Fig. 2.

No.		Element			
		Fe	As	Cl	O
(a)	Wt%	32	27	8	33
	At%	17	11	7	65
(b)	Wt%	24	20	7	49
	At%	11	7	5	77
(c)	Wt%	27	27	7	39
	At%	14	10	6	70
(d)	Wt%	27	25	7	41
	At%	14	9	6	71
(e)	Wt%	39	28	9	24
	At%	25	13	9	53

Wt%: weight percentage; At%: atomic percentage.

In the absence of SO_4^{2-}, the Raman band of crystalline ferric arsenite hydroxychloride at 448 cm^{-1} was considered to be assigned to As–O out-of-plane bending vibration or Fe–O bending vibration. However, the band at 610 cm^{-1} was only probably attributed to the Fe–O vibration (Müller et al., 2010). Compared to the band observed at 780 cm^{-1} on the Raman spectrum of tooeleite, it can be observed that the As(III)–O stretching vibration band of crystalline ferric arsenite hydroxychloride shifted towards the higher wave number (806 cm^{-1}). This indicated that the band was only ascribed to As(III)–O symmetric stretching vibrations. Compared with tooeleite, a new weaker band at 961 cm^{-1} emerged in crystalline ferric arsenite hydroxychloride. Müller et al. (2010) also indicated that this band was originated from As–O stretching vibrations. Like tooeleite, the band of crystalline ferric arsenite hydroxychloride at 661 cm^{-1} was assigned to As(III)–OH stretching vibration. The above-mentioned results suggested that both chlorine and arsenite filled the positions of sulfate association with Fe to from ferric arsenite hydroxychloride. Similar to the crystal structure of tooeleite, Cl probably

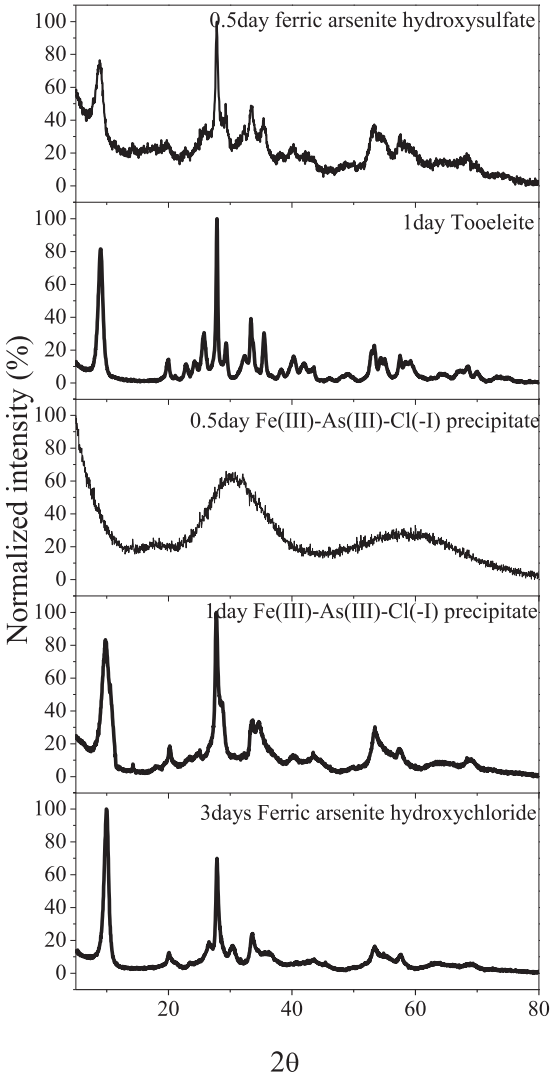

Fig. 3 – The time-varying X-ray diffraction (XRD) patterns of Fe(III)–As(III)–Cl(-I) precipitates produced at pH 2.3 and reference materials (ferric arsenite hydroxysulfate and tooeleite).

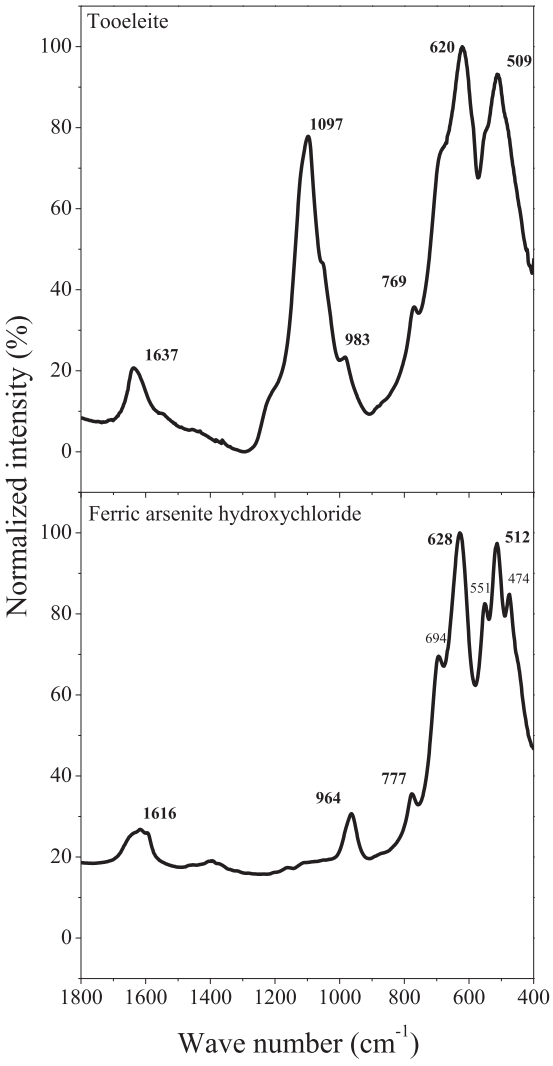

Fig. 4 – Comparison of infrared spectra (FT-IR) of the Fe(III)–As(III)–Cl(-I) precipitate produced at pH 2.3 with tooeleite.

entered the intercalated layers involving AsO_3 pyramids bonded to FeO_6 octahedra by both edge- and corner-linkage in crystalline ferric arsenite hydroxychloride.

2.2.5. *TG analysis*

Fig. 6 shows the TG curve for the precipitate produced at pH 2.3 after the reaction of As(III) with Fe(III) in chloride solution. Ferric arsenite hydroxychloride displayed weight loss (5%) at the beginning of the test on the TG curve, which was reasonably attributed to the removal of adsorbed water according to the natural drying treatment of the fresh sample in the anaerobic glove box under N_2. The first weight loss step was reached to 10.49% due to the release of five crystallization water, indicating the formula of ferric arsenite hydroxychloride: $Fe_5(AsO_3)_3Cl_2(OH)_4 \cdot 5H_2O$. This number (10.49%) was close with water content (10.41%, 9.26% × 18/16) according to the O content of H_2O (11.77%) as indicated by EDS data. The O content of AsO_3 and OH (15.92% and 7.07%) from the mean O content of ferric arsenite hydroxychloride (32.25% = 37.25%–5%) equals the O content of H_2O (9.26%). Hence, the expected overall reaction can be written as Eq. (1)

$$5FeCl_3 + 3H_3AsO_3 + 9H_2O \rightarrow Fe_5(AsO_3)_3Cl_2(OH)_4 \cdot 5H_2O + 13HCl \quad (1)$$

The weight of solid sample continued to decrease until reach the stable state again in the temperature range 600–800°C (1.99% weight loss), suggesting that the weight lose could be partly due to the sublimation of As_2O_3 (Nishimura and Robins, 2008). Furthermore, 0.1 g of Fe(III)–As(III)–Cl(-I) precipitate produced at pH 2.3 in this work was completely dissolved with 10 mL 6 moL/L HCl solution. The concentrations of dissolved Fe, As and Cl were 3104.2, 2540.8 and 788.7 mg/L with Fe:As:Cl molar ratio of 5: 3: 2, which was very close to the theoretical value (Fe 3189.1 mg/L, As 2562.8 mg/L

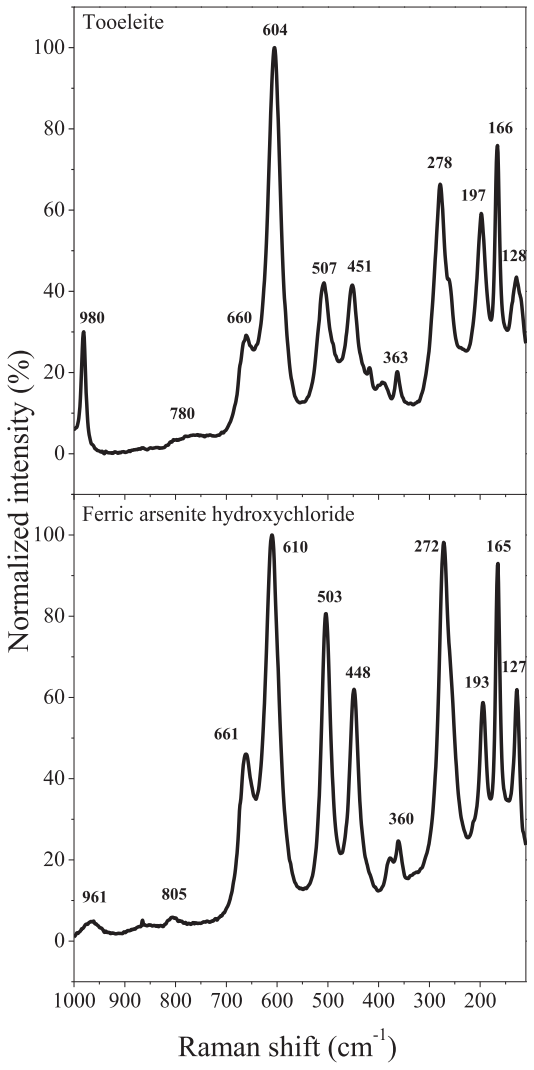

Fig. 5 – Comparison of Raman spectra of the Fe(III)–As(III)–Cl(-I) precipitate produced at pH 2.3 with tooeleite.

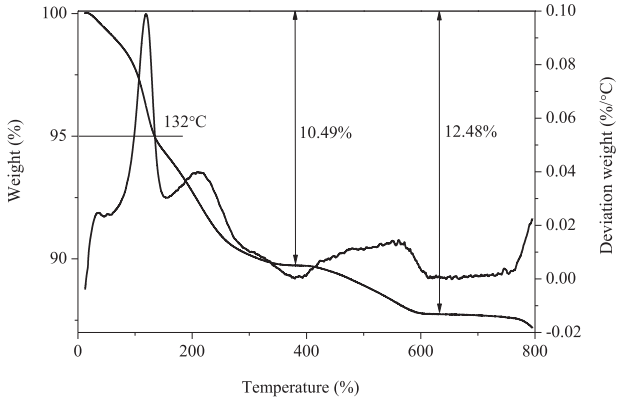

Fig. 6 – Thermogravimetric analysis of the precipitate produced at pH 2.3.

and Cl 808.7 mg/L). It further indicated that $Fe_5(AsO_3)_3Cl_2(OH)_4 \cdot 5H_2O$ was very likely the chemical formula of the obtained precipitate at pH 2.3. According to the results of solid-phase characterization together with the time-varying color of the obtained Fe(III)–As(III)–Cl(-I) precipitate from orange to yellow (Appendix A Fig. S4), the pathway of the $Fe_5(AsO_3)_3Cl_2(OH)_4 \cdot 5H_2O$ formation, which was similar to that of tooeleite formation, was likely to be described as follows. The co-precipitation of As(III) with Fe(III) occurred at pH 2.3. Cl(-I) subsequently incorporated the intercalated layers in AsO_3 pyramids bonded to FeO_6 octahedra for the formation of amorphous ferric arsenite hydroxychloride to further convert to crystalline $Fe_5(AsO_3)_3Cl_2(OH)_4 \cdot 5H_2O$.

2.3. *Effect of Cl(-I) on as and Fe removal in aqueous sulfate media*

As and Fe removal efficiencies in aqueous sulfate media were compared with those in aqueous sulfate-chloride media after 3-day reaction at pH 1.6–9.5 (Fig. 7). A little precipitate was formed from pH 1.9 in sulfate-chloride solution (Appendix A Fig. S1c). This was different from the results in sulfate or chloride media (Appendix A Figs. S1a–b), indicating that a lower solubility ferric arsenite phase at acid pH conditions probably acted as a new As sink. It was obvious that As and Fe removal efficiencies at pH 2.3–2.6 and 4.5–5.3 in the presence of Cl(-I) were higher. At pH 2.3–2.6, As and Fe removal efficiencies in aqueous sulfate-chloride media were 17% and 11%–17% higher than those in aqueous sulfate media. It indicated that the addition of Cl(-I) could contribute to more As(III) association with more Fe(III), causing the probable formation of sulfate-chloride ferric arsenite according to the presence of excessive sulfate in the initial system and higher solubility of ferric arsenite hydroxychloride.

A decrease of As removal efficiency occurred at pH range 3–7, although the overall trend of As removal efficiency increased with the increase pH in two systems. This was similar to the previous work in aqueous sulfate media (Chai

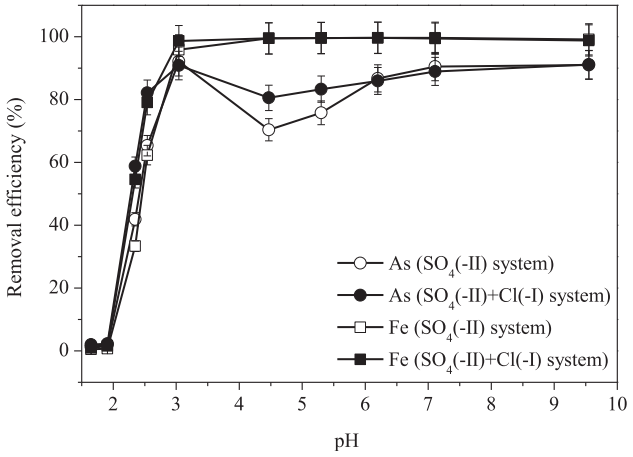

Fig. 7 – As(III) and Fe(III) removal efficiency at various pH values after the precipitation reaction of As(III) with Fe(III) in aqueous sulfate and sulfate-chloride media. Data are represented as averages ± standard deviation.

et al., 2016), which was explained that arsenite cannot adsorbed on or co-precipitated with sulfate-ferrihydrite at Fe/As molar ratio of ≤2 under slightly acidic pH conditions (Ona-Nguema et al., 2005) and sulfate competed with arsenite for similar adsorption sites (Jia and Demopoulos, 2005), leading to more As remaining. At pH 4.5–5.3, the differences of As removal efficiency were 10.2% and 7.5% between two systems, despite almost all of Fe removal efficiency, which was reasonably attributed to the presence of more sulfate-chloride ferric arsenite than tooeleite in respective systems. It was also found indirectly that the color of the slurry in sulfate-chloride system was still yellow at pH 4.5. However, the content of this precipitate decreased as increasing pH according to the formation of the reddish brown slurry at pH 5.3. Hence, the gap of their pure technical efficiency in two systems is continuously narrow.

The addition of Cl(-I) into aqueous sulfate media for the precipitation of As(III) with Fe(III) salts played a key role in the removal of soluble As. Sulfate-chloride ferric arsenite as the main solid has lower solubility, causing an increase in As immobilization. Therefore, it would be useful to introduce Cl(-I) into aqueous As(III)-rich sulfate media including hydrometallurgical effluents or acid mine drainage for effective As removal under acidic conditions, in order to decrease the usage of neutralizing reagents.

2.4. *Discussion*

Cl(-I) participates in mineral composition is an important process influencing the mobility of arsenite or iron in nature and mining related environments (Maithreepala and Doong, 2005; Bahfenne and Frost, 2010; Alidokht et al., 2016). To date, little attention has been paid to the relationship among Fe(III), As(III) and Cl(-I), although As(III) may associated with the two as a new sink for the fixation of As(III). It only exists limited examples in hydrometallurgical effluents or acid mine drainage on the formation of ferric arsenite hydroxysulfate for direct As(III) removal (Chai et al., 2016, 2018).

To address this issue, mixed Fe(III)–As(III)–Cl(-I) solutions are neutralized to different various pH for a new precipitate. It is found that Cl(-I) instead of SO_4(-II) as a main component associates with As(III) and Fe(III) at pH 2.3 for the formation of crystalline ferric arsenite hydroxychloride ($Fe_5(AsO_3)_3Cl_2(OH)_4\cdot 5H_2O$) compared with tooeleite, causing the immobilization of As(III). The concentrations of As leached from synthetic $Fe_6(AsO_3)_4SO_4(OH)_4\cdot 4H_2O$ and $Fe_5(AsO_3)_3Cl_2(OH)_4\cdot 5H_2O$ in this study are 30 mg/L and 32 mg/L, respectively (Appendix A Fig. S5), which are similar and both exceed the regulatory limit (As 5 mg/L). This precipitation method can be employed to directly remove soluble As(III) in chloridizing leaching media originated from metal recovery. Unfortunately, the solubility of $Fe_5(AsO_3)_3Cl_2(OH)_4\cdot 5H_2O$ is higher than that of $Fe_6(AsO_3)_4SO_4(OH)_4\cdot 4H_2O$. However, the addition of Cl(-I) in sulfate solution is determined for enhancing As(III) removal efficiency via the formation of sulfate-chloride ferric arsenite under acidic pH conditions. This finding shows the existence of $Fe_5(AsO_3)_3Cl_2(OH)_4\cdot 5H_2O$ and provides a novel method for enhancing As removal from hydrometallurgical effluents or acid mine drainage at pH range 2–3.

At pH 2.3, raising the temperature is not conducive to the formation of ferric arsenite hydroxychloride. The final solids of As(III) with Fe(III) in aqueous chloride media at pH 2.3 under different temperatures (40 °C, 60 °C and 80 °C) for 3 days are characterized by XRD and their patterns are compared with those of the reference materials (ferric arsenite hydroxychloride, Fe(III)–As(III)–Cl(-I) precipitate and As(III)-bearing ferrihydrite) in Appendix A Fig. S6. The crystallinity of ferric arsenite hydroxychloride on the XRD patterns decrease with increasing temperature from 40 to 60 °C until all the ferric arsenite hydroxychloride features disappear at 80 °C. There are also some features of amorphous phase on the XRD patterns at 40 and 60 °C. The amorphous level of final solids on the XRD patterns gradually increases from 40 to 80 °C. At 80 °C, the two broad bands of the reaction product at 34° and 60° 2θ are obscured by the characteristic diffraction bands of As(III)-bearing ferrihydrite. Three reaction products vary in color from orange to red brown with increasing temperature (Appendix A Fig. S7). It indicates that the mixture of ferric arsenite hydroxychloride and As(III)-bearing ferrihydrite may be formed at 40 and 60 °C. The reason might be that the pH (2.3) for the precipitation is closer to the pH (2.6) for the obvious Fe(III) hydrolysis and the increase in temperature can promote Fe(III) hydrolysis (Stefansson et al., 2007). Therefore, near room temperature is more suitable for the formation of ferric arsenite hydroxychloride. The use of Cl(-I) on the As(III) precipitation with Fe(III) in the wastewater treatment process can save the heating energy consumption.

3. Conclusions

Three major findings are:(1) A yellow precipitate was produced after 3-days reaction with Fe(III)/As(III) molar ratio 1.7 in chloride solution at neutralized pH 2.3. Chemical analysis together with solid characterization including SEM-EDS, XRD, FTIR, Raman and TG indicated that compared with the chemical composition of tooeleite, SO_4(-II) was replaced by Cl(-I) forming crystalline ferric arsenite hydroxychloride ($Fe_5(AsO_3)_3Cl_2(OH)_4\cdot 5H_2O$). (2) The ferric arsenite hydroxychloride showed tiny plate shaped crystallites and its XRD, FT-IR and Raman bands were similar to those of tooeleite. The characteristic bands of crystalline ferric arsenite hydroxychloride occurred at 10°, 20°, 26°, 28°, 30°, 33°, 36°, 43°, 53°, 57° 2θ for XRD, 474, 512, 551, 628, 694, 777, 964, 1616 cm^{-1} for FT-IR and 127, 165,193, 272, 360, 448, 503, 601, 661, 805 and 961 cm^{-1} for Raman spectra. (3) The addition of Cl(-I) into aqueous sulfate media significantly increased As removal efficiency in the pH range 2.3–2.6 and 4.5–5.3, although the solubility of ferric arsenite hydroxychloride was lower than that of tooeleite. Sulfate-chloride ferric arsenite was very likely to be a new sink for the fixation of As(III) from hydrometallurgical effluents or acid mine drainage under acidic pH conditions.

Acknowledgments

This work was supported by the National Natural Science Foundation of China (Nos. 41530643, 41703133 and 41877393),

the Chinese Academy of Sciences (No. QYZDJSSW-DQC038) and the Liaoning Province Doctoral Scientific Research Initiation Fund Project (No. 2019-BS-261).

Appendix A. Supplementary data

Supplementary data to this article can be found online at https://doi.org/10.1016/j.jes.2019.12.009.

REFERENCES

Alidokht, L., Oustan, S., Khatee, A., Neyshabouri, M.R., Reyhanitabar, A., 2016. Enhanced removal of chromate by graphene-based sulfate and chloride green rust nanocomposites. J. Taiwan Inst. Chem. E. 68, 266–274.

Azamat, J., Khataee, A., Sadikoglu, F., 2018. Computational study on the efficiency of MoS_2 membrane for removing arsenic from contaminated water. J. Mol. Liq. 249, 110–116.

Bahfenne, S., Frost, R.L., 2010. Raman spectroscopic study of the mineral finnemanite $Pb_5(As^{3+}O_3)_3Cl$. J. Raman Spectrosc. 41, 329–333.

Cai, G., Zhu, X., Li, K., Qi, X., Wei, Y., Wang, H., et al., 2019. Self-enhanced and efficient removal of arsenic from waste acid using magnetite as an in situ iron donator. Water. Res. 157, 269–280.

Chai, L., Yue, M., Li, Q., Zhang, G., Zhang, M., Wang, Q., et al., 2018. Enhanced stability of tooeleite by hydrothermal method for the fixation of arsenite. Hydrometallurgy 175, 93–101.

Chai, L., Yue, M., Yang, J., Wang, Q., Li, Q., Liu, H., 2016. Formation of tooeleite and the role of direct removal of As(III) fromhigh-arsenic acid wastewater. J. Hazard. Mater. 320, 620–627.

Frost, R., Martens, W., Williams, P., Kloprogge, J., 2003. Raman spectroscopic study of the vivianite arsenate minerals. J. Raman Spectrosc. 34, 751–759.

Gotić, M., Musić, S., 2007. Mössbauer FT-IR and FE SEM investigation of iron oxides precipitated from $FeSO_4$ solutions. J. Mol. Struct. 834–836, 445–453.

Halder, D., Lin, J., Essilfie-Dughan, J., Das, S., Robertson, J., Hendry, M.J., 2018. Implications of the iron(II/III)-arsenic ratio on the precipitation of iron-arsenic minerals from pH 2.5 to 10.5. Appl. Geochem. 98, 367–376.

Jain, A., Loeppert, R.H., 2000. Effect of competing anions on the adsorption of arsenate and arsenite by ferrihydrite. J. Environ. Qual. 29, 1422–1430.

Jia, Y., Demopoulos, G.P., 2005. Adsorption of arsenate onto ferrihydrite from aqueous solution: influence of media (sulfate vs nitrate), added gypsum, and pH alteration. Environ. Sci. Technol. 39, 9523–9527.

Kobya, M., Soltani, R.D.C.S., Omwene, P.I., Khataee, A., 2020. A review on decontamination of arsenic-contained water by electrocoagulation: Reactor configurations and operating cost along with removal mechanisms. Environ. Technol. Inno. 17, 100519.

Ledderboge, F., Metzger, S.J., Heymann, G., Huppertz, H., Schleid, T., 2014. Dimorphic cerium(III) oxoarsenate(III) Ce $[AsO_3]$. Solid State Sci 37, 164–169.

Liu, J., Cheng, H., Frost, R.L., Dong, F., 2013. The mineral tooeleite $Fe_6(AsO_3)_4SO_4(OH)_4\cdot 4H_2O$ – An infrared and Raman spectroscopic study environmental implications for arsenic remediation. Spectrochim. Acta A 103, 272–275.

Ma, X., Gomez, M.A., Yuan, Z., Zhang, G., Wang, S., Li, S., et al., 2019. A novel method for preparing an As(V) solution for scorodite synthesis from an arsenic sulphide residue in a Pb refinery. Hydrometallurgy 183, 1–8.

Maithreepala, R.A., Doong, R.-A., 2005. Enhanced dechlorination of chlorinated methanes and ethenes by chloride green rust in the presence of copper(II). Environ. Sci. Technol. 39, 4082–4090.

Majzlan, J., Dachs, E., Benisek, A., Koch, C.B., Bolanz, R., Göttlicher, J., et al., 2016. Thermodynamic properties of tooeleite, $Fe_6^{3+}(As^{3+}O_3)_4(SO_4)(OH)_4\cdot 4H_2O$. Chem. Erde-Geochem. 76, 419–428.

Makreski, P., Stefov, S., Pejov, L., Jovanovski, G., 2015. Theoretical and experimental study of the vibrational spectra of (para) symplesite and hörnesite. Spectrochim. Acta A 144, 155–162.

Michelis, I.D., Olivieri, A., Ubaldini, S., Ferella, F., Beolchini, F., Vegliò, F., 2013. Roasting and chlorine leaching of goldbearing refractory concentrate: experimental and process analysis. Int. J. Min. Sci. Technol. 23, 709–715.

Morin, G., Juillot, F., Casiot, C., Bruneel, O., Personné, J.-C., Elbaz-Poulichet, F., et al., 2003. Bacterial formation of tooeleite and mixed arsenic(III) or arsenic(V)-iron(III) gels in the Carnoule's acid mine drainage, France. A XANES, XRD, and SEM study. Environ. Sci. Technol. 37, 1705–1712.

Müller, K., Ciminelli, V.S.T., Dantas, M.S.S., Willscher, S., 2010. A comparative study of As(III) and As(V) in aqueous solutions and adsorbed on iron oxy-hydroxides by Raman spectroscopy. Water. Res. 44, 5660–5672.

Nishimura, T., Robins, R.G., 2008. Confirmation that tooeleite is a ferric arsenite sulfate hydrate, and is relevant to arsenic stabilisation. Miner. Eng. 21, 246–251.

Nur, T., Loganathan, P., Ahmed, M.B., Johir, M.A.H., Nguyen, T.V., Vigneswaran, S., 2019. Removing arsenic from water by coprecipitation with iron: Effect of arsenic and iron concentrations and adsorbent incorporation. Chemosphere 226, 431–438.

Okibe, N., Koga, M., Morishita, S., Tanaka, M., Heguri, S., Asano, S., et al., 2014. Microbial formation of crystalline scorodite for treatment of As(III)-bearing copper refinery process solution using Acidianus brierleyi. Hydrometallurgy 143, 34–41.

Ona-Nguema, G., Morin, G., Juillot, F., Calas, G., Brown Jr., G.E., 2005. EXAFS analysis of Arsenite adsorption on two-line ferrihydrite, hematite, goethite, and lepidocrocite. Environ. Sci. Technol. 39, 9147–9155.

Peulon, S., Legrand, L., Antony, H., Chaussé, A., 2003. Electrochemical deposition of thin films of green rusts 1 and 2 on inert gold substrate. Electrochem. Commun. 5, 208–213.

Priestner, M., Singer, G., Weil, M., Kremer, R.K., Libowitzky, E., 2019. Synthesis, structural, magnetic and thermal properties of Mn2As2O5, the first pyro-arsenite of a first-row transition metal. J. Solid State Chem 277, 209–215.

Revesz, E., Fortin, D., Paktunc, D., 2016. Reductive dissolution of arsenical ferrihydrite by bacteria. Appl. Geochem. 66, 129–139.

Sancho-Tomás, M., Somogyi, A., Medjoubi, K., Bergamaschi, A., Visscher, P.T., Van Driessche, A.E.S., et al., 2018. Distribution, redox state and (bio)geochemical implications of arsenic in present day microbialites of Laguna Brava, Salar de Atacama. Chem. Geol. 490, 13–21.

Stefansson, A., 2007. Iron(III) hydrolysis and solubility at 25°C. Environ. Sci. Technol. 41, 6117–6123.

Xiao, F., Wang, S., Xu, L., Wang, Y., Yuan, Z., Jia, Y., 2015. Adsorption of monothioarsenate on amorphous aluminum hydroxide under anaerobic conditions. Chem. Geol. 407–408, 46–53.

Yew, Y.P., Shameli, K., Miyake, M., Kuwano, N., Khairudin, N.B.B.A., Mohamad, S.E.B., et al., 2016. Green synthesis of magnetite (Fe_3O_4) nanoparticles using seaweed (*Kappaphycus alvarezii*) extract. Nanoscale Res. Lett. 11, 1–7.

Yuan, Z., Zhang, G., Ma, X., Yu, L., Wang, X., Wang, S., et al., 2019. Rapid abiotic As removal from As-rich acid mine drainage: Effect of pH, Fe/As molar ratio, oxygen, temperature, initial As

concentration and neutralization reagent. Chem. Eng. J. 378, 122156.
Zhang, T., Zhao, Y., Kang, S., Li, Y., Zhang, Q., 2019. Formation of active $Fe(OH)_3$ in situ for enhancing arsenic removal from water by the oxidation of Fe(II) in air with the presence of $CaCO_3$. J. Clean. Prod. 227, 1–9.
Zhang, W., Singh, P., Issa, T.B., 2011. Arsenic(III) remediation from contaminated water by oxidation and Fe/Al co-precipitation. J. Water Resour. Pollut. 3, 655–660.
Zhou, S., Wei, Y., Li, B., Wang, H., Ma, B., Wang, C., 2016. Chloridization and reduction roasting of high-magnesium low-nickel oxide ore followed by magnetic separation to enrich ferronickel concentrate. Mater. Trans. 47B, 145–153.